Journal of
Chemical Engineering & Process Technology

Pérez et al., J Chem Eng Process Technol 2018, 9:1
DOI: 10.4172/2157-7048.1000374

Research Article Open Access

Use of Multivariable Analysis (ANOVA) to Compare Irradiation Sources on Diuron Destruction by Photocatalysis Using TiO_2-P25 Impregnated with Sm^{3+}, Eu^{3+} and Gd^{3+}

Juan Carlos Arévalo Pérez[1,2], Jose Gilberto Torres[1]*, Adrian Cervantes Uribe[1], Hermicenda Pérez Vidal[1], Adrian Cordero García[1], Armando Izquierdo Colorado[2,3], Adib Abiu Silahua Pavón[1] and Wilfrido Miguel Contreras Sánchez[2]

[1]*Laboratory of Catalytic Nanostructures, Applied Science and Technology Research Center of Tabasco (CICTAT), Universidad Juárez Autónoma de Tabasco, Mexico*
[2]*División Académica de Ciencias Biológicas, Universidad Juárez Autónoma de Tabasco, Mexico*
[3]*Jean-Rond d'Alembert Institute, Sorbonne University, France*

Abstract

Ions of Sm^{3+}, Eu^{3+} and Gd^{3+} were deposited onto the surface of TiO_2-P25 using an impregnation method, and the catalysts were calcined to 500°C in order to provide thermal stability to the crystalline phases. A sample of pure P25 was processed under the same synthesis conditions. The materials were characterized by physisorption of N_2, X-ray diffraction and Scanning Electron Microscope and Spectroscopy UV-Vis with diffuse reflectance. It was observed by SEM that P25 had an amorphous surface forming irregular aggregates and deformations in which the studied lanthanide ions were inserted. Due to heat treatment, the P25 suffered modifications that showed a higher photocatalytic activity in the visible region, by the presence of oxygen vacancies generated by the removal of impurities (C and Cl). XRD analyses determined the distribution and crystal size of the crystalline phases presented in the P25 (anatase and rutile). Lanthanide ions possibly demonstrated an effect of superficial coalescing in the rutile phase of the P25. A completely randomized experimental design was used to determine the catalytic evaluation, and sunlight was statistically shown to be the best condition for the degradation and mineralization of diuron. Comparing treatments indicated a better option: using the catalyst with 0.3 wt% Gd under sunlight.

Keywords: ANOVA; Irradiation source; Photocatalysis; Diuron; TiO_2-P25

Introduction

In recent years, human consumption of water has increased dramatically, especially for use in agriculture. Along with this increase has come the excessive use of pesticides, most of which are chemicals that are difficult to remove and are poured onto the soil and drained into aquatic systems, making it difficult to obtain clean water. Diuron is one such pesticide that causes this problem; it is used as a pre-emergent herbicide to control annual broadleaf dicotyledonous weeds [1]. This compound is toxic to all living beings. It causes birth defects, is carcinogenic and cannot be removed when it is applied in high doses to the ground. Due to excessive use and low volatility, it has an environmental biodegradation of longer than 300 days [2]. This compound is often found in surface water and groundwater [3,4], and its main forms of transport in the environment are through urban runoffs and agricultural activity. Another source of contamination arises from washing the containers of herbicide before their disposal, and in these instances the diuron concentration exceeds that found in natural effluents. The European Union Water Framework Directive considers its toxicity a priority and limits the use of this pesticide as a hazardous substance [5,6].

Because of this classification, chemical [7], physical [8] and biological [9] efforts have been made to eliminate this herbicide. Chemical methods are the most efficient in the removal of this pollutant, and among them, the advanced oxidation processes (AOPs) stand out. These processes include heterogeneous photocatalysis with TiO_2, which efficiently eliminates persistent organic pollutants (POPs) by oxidizing these compounds to CO_2 without producing secondary compounds of high toxicity [10]. This process requires the use of a semiconductor, such as TiO_2, to generate electron-hole pairs (e^-, h^+) able to produce hydroxyl radicals (OH^*) responsible for catalytic oxidation of a wide range of POPs. Unfortunately, TiO_2 exhibits spectral response only under UV light, has low quantum efficiency and a high speed of recombination of pairs e^--h^+, which inhibits its photocatalytic activity [11].

Recently, research has been devoted to the study, modification and composition of titania, with the aim of obtaining a solid photocatalyst that has a spectral response in the ultraviolet and visible region. To achieve this end, its internal and external structure has been modified by adding metallic and nonmetallic impurities in low concentrations (doping). Recently, rare earth ions, or lanthanides, have attracted attention because they may increase the physicochemical and photocatalytic properties of TiO_2. These ions offer advantages in the absorption of light corresponding to the visible region; studies with these metals are focused on their luminescent properties when housed in crystalline matrices. These ions also have the ability to form complexes with various Lewis bases due to the interaction of these functional groups with the f orbitals. These play an important role in increasing the photocatalytic activity of TiO_2 by removing contaminants on its surface [12]. It has been reported that incorporation of trivalent ions of rare earth elements (La, Ce, Er, Pr, Gd, Nd and Sm) in the titania using

***Corresponding author:** Torres G, Laboratory of Catalytic Nanostructures, Applied Science and Technology Research Center of Tabasco (CICTAT), Universidad Juárez Autónoma de Tabasco, Mexico, Tel: +529933581500; E-mail: torremensajes@gmail.com

Received January 20, 2018; **Accepted** February 09, 2018; **Published** February 20, 2018

Citation: Pérez JCA, Torres JG, Uribe AC, Vidal HP, García AC, et al. (2018) Use of Multivariable Analysis (ANOVA) to Compare Irradiation Sources on Diuron Destruction by Photocatalysis Using TiO^2-P25 Impregnated with Sm^{3+}, Eu^{3+} and Gd^{3+}. J Chem Eng Process Technol 9: 374. doi: 10.4172/2157-7048.1000374

the sol-gel method shows an increase in the photocatalytic activity of TiO_2 when 0.5 wt% to 1 wt% of rare earth elements is used. Addition of 1 wt% Gd^{3+} showed a much higher activity than untouched TiO_2-P25 [13]. However, the sol-gel method is not the only way to dope trivalent rare earth ions into TiO_2. La^{3+}, Pr^{3+} and Nd^{3+} ions have been deposited onto the surface of titania using the impregnation method by varying the amount of dopant metals as 0.3 wt%, 0.5 wt%, 0.8 wt% and 1 wt%. Under these conditions, 0.5% wt La^{3+} showed the best morphology and photocatalytic properties under sunlight in the degradation of methylene blue [14]. Therefore, for this study, TiO_2-P25 was doped to 3 wt% and 5 wt% with Sm^{3+}, Eu^{3+} and Gd^{3+} ions by the impregnation method to improve morphological properties electronically. The dopants were also studied in lower concentrations to determine whether the photocatalytic activity of TiO_2-P25 would still be improved. Because the photocatalytic evaluation was being performed with sunlight, the dopants were also studied in lower concentrations to determine whether the photocatalytic activity of P25 still improved.

Experimental

Reagents

Diuron, (3-(3,4-dichlorophenyl)-1, 1-dimethylurea) >98% Sigma-Aldrich brand, was used as aqueous contaminant. The precursors of the impregnated metals used were nitrates of samarium, europium and gadolinium with a purity >99.9% (Sigma-Aldrich). The TiO_2-P25 was obtained from Evonik-Degussa Corp. The water used in the experiments was obtained from a Purelab option Q7BP purifier, which reflected a resistivity >18 MΩcm to room temperature.

Catalysts

The metal ions were incorporated into the surface of P25 in two different concentrations, 0.3 wt% and 0.5 wt%, using the impregnation method. The precursor salts were dissolved in one tenth of the volume of water used. Subsequently, the precursor metal solution was mixed with P25 and stirred for 4 h at ambient temperature, and then the excess water was removed using a rotary evaporator at 70°C. The resultant solid was dried for 12 h at 120°C and calcined for 6 h at 500°C with a heating ramp of 2°C min^{-1}. All pure P25 was generated in this manner to ensure equal conditions in all experiments.

Characterization

Physisorption of nitrogen

The characterization of surface areas and porosimeter systems was performed with "Micromeritics Instrument Corporation" model Tristar II 3020. Samples were degassed at 350°C for 2 h prior to analysis.

X-Ray Diffraction (XRD)

An X-ray diffractometer Bruker model D8 advance was used to obtain the crystallographic planes of the crystal structures in the samples; they were identified through the library of the Joint Committee on Powder Diffraction Control Standards (JCPDS). The crystal size was calculated in nm (D) of the crystalline phases with Eq. (1) [15]:

$$D = \frac{K\lambda'}{\beta Cos\theta} \quad (1)$$

The percentage of the Rutile phase (%R) at the TiO_2-P25 was determined using Spurr Equation (2) [16]:

$$\%R = \left(\frac{1}{1+\left(0.8\times\frac{I_A}{I_R}\right)}\right)\times 100 \quad (2)$$

UV-Vis spectroscopy with diffuse reflectance

UV-Vis spectra were used to estimate the band gap energy (E_g) for each catalyst, if the absorption coefficient (α) is zero, according to equation (3). This was performed in a UV-Vis spectrophotometer equipped with an integrating sphere for diffuse reflectance (Varian model Cary 300) using $BaSO_4$ as a reference.

$$a(\mathrm{hv}) = \mathrm{A}(\mathrm{hv} - \mathrm{E_g})^{\frac{m}{2}} \quad (3)$$

Scanning Electron Microscopy (SEM)

A scanning electron microscope JEOL model JSM-6010LA was used to identify in detail the surface morphology of the catalysts. The analyzer XEDS (X-Ray Energy Dispersive Spectrometry) was used to identify the impurities present in the TiO_2-P25 before and after heat treatment.

Photocatalytic activity

Determination of catalytic efficiency in the photocatalytic degradation and mineralization of diuron was performed in aqueous medium at 40 mgL^{-1} (water solubility). At this concentration, diuron showed a pH of 5.5 and an initial content of the total organic carbon (TOC) of 20.35 mg of CL^{-1}. This compound in an aqueous medium showed a maximum absorbance at 248 nm. For all the experiments, 5 L of aqueous diuron was prepared by dissolving it in a container with no light under constant stirring for 72 h at ambient temperature. The reactions were developed on a borosilicate Ace photocatalytic reactor that was enabled with a quartz recirculation system to maintain a constant reaction temperature of 20°C. It had a total volume of 500 ml with side entrances, through which were supplied a constant flow of 60 $mlseg^{-1}$ atmospheric O_2 and a collecting hose for taking reaction samples. The catalyst concentration was 0.5 gL^{-1}, which reached the equilibrium of the diuron solution previous to the reaction. The total reaction time was 300 min. For reactions carried out under sunlight, the fully equipped reactor was placed on the roof of the laboratory building in full sunlight from 10:00 a.m. to 3:00 p.m. The intensity of sunlight was monitored during reactions with a radiometer NR-LITE Net and was measured at intensity between 2.7 and 3.0 Wcm^{-2} with a sensitivity of 10 $\mu VW^{-1}m^2$. UV reactions were performed in a fume hood that was completely covered to prevent the passage of the external light and using a mercury lamp with an intensity of 1,800 μWcm^{-2} and a 254 nm UV light source. For both light conditions, the stirring, the atmospheric O_2 flow and the temperature were constants, and samples were taken every 60 min. The catalyst was removed using a membrane filter of 0.25 µm. The degradation process was monitored by UV-Vis spectroscopy by taking the diuron's maximum absorbance measurement. The mineralization was determined by the total catalytic combustion of organic matter through a total organic carbon analyzer Shimadzu Model TOC-VCSN.

Experimental Design

We developed a completely randomized design (2 × 2 × 3) to determine the larger factors impacting the photocatalytic removal of diuron. These factors were established as lighting mode (solar and UV), type of metal impregnated on the P25 (Sm, Eu and Gd) and concentration of impregnated metal (0.3 wt% and 0.5 wt%). However, there were two additional treatments in the design that were taken as witnesses (solar and UV) and kept the same in each reaction condition post treatments. Overall 14 treatments repeated three times each generated 42 data points. The oxidation rate and the percentage of mineralization were used as a response variable and were monitored

every 60 min for up to approximately 300 min for each treatment.

The data generated from these experiments were pooled according to initial concentration. These 252 data points were used to compare regression lines for each treatment. Using the reply-percentage variable of the oxidation, the reaction rate constant *"k"* was determined for each treatment, while a pseudo-constant was determined using the percentage to establish the conditions in which the mineralization was carried out more efficiently.

Results and Discussion

Characterization

It is known that TiO_2-P25 does not have a porous structure when compared with TiO_2 in its 100% anatase phase or with other metal-oxide-semiconductors [17]. The images obtained by SEM showed that TiO_2-P25 has an amorphous surface with irregular aggregates forming imperfections on the P25 surface where the lanthanide ions were deposited. Figure 1 shows the images of TiO_2-P25 calcined at 500°C (a) and TiO_2-P25 without heat treatment (b). Both images reveal no uniform shapes or patterns for the TiO_2-P25, only winding surfaces with irregularities that have a specific area close to the reported in the literature. The image of the sample treated at 500°C exhibits a less amorphous surface that the image presented in subsection b). Table 1 shows the results of the characterizations carried out on the catalysts. The P25-specific area increased because of the presence of 0.3 wt% Gd^{3+} and slightly increased with 0.5 wt% Sm^{3+} due to the high metal dispersion that generated higher deformations. However, other impregnated ions showed values closer to those reported by the manufacturer of the P25 [18].

XRD analysis showed similarity between the samples. It was observed that all of the catalysts have mixtures of crystalline phases (anatase and rutile), and the impregnated ions did not reflect any characteristic signal (Figure 2) due to the small amount of impregnated metal; similar cases have been reported in studies of lanthanide ions doped into TiO_2-P25 [19]. The distribution of the crystalline phases in Table 1 was modified due to the heat treatment that the catalysts underwent. Just as impurities were added and their concentration increased, the TiO_2-P25 obtained the distribution previously reported [18].

The results obtained for the average crystal size of each crystal phase are shown in Table 1. The Anatase phase showed values between 21 and 26 nm, which remained the same after impregnation, and this value is lower than that previously reported (37 nm) [20]. This decrease is mainly due to the high calcination temperature that generated a nucleating effect on the crystals. Only the sample with 0.3 wt% Gd^{3+} increased 5 nm, but increasing the amount of metal stabilized the crystal size. This demonstrates that the dispersion of this ion at this concentration was expressed mainly in the anatase phase, leaving the rutile phase stable. Therefore, the sample had higher surface deformation in the most abundant crystalline phase, increasing its surface area.

A crystal size for the rutile phase of approximately 35 nm had previously been reported for P25 that had been impregnated with Pt [21], Ag [22], La, Ce, Y, Pr and Sm [19], and increasing the concentrations of these metals stabilized the crystal sizes for both phases. In this study, the crystal size for the rutile phase was possibly higher due to oxygen vacancies and to rearrangement caused by the thermal treatment used to remove impurities from P25. However, increasing the concentration of ions in the rutile crystals decreased 17 nm, indicating that the Ti-OM (M=Sm, Eu and Gd) bonds on the P25 surface formed by coalescence during the thermal treatment were selective for rutile phase (for a few samples), likely due to the stability that this phase has relative to the anatase phase. It was observed that 0.3 wt% Gd^{3+} did not change the rutile crystal size, due to the selectivity that the metal has for the anatase phase.

The diffuse reflectance spectra are shown in Figure 3. It was observed that the P25 absorption band is displaced to longer wavelengths (>400 nm) corresponding to visible light. Although the catalysts showed a white coloration, this absorption is due to the electronic transition that the 2*p* orbital of O undergoes to the Ti 3d orbital, which the theory of "ligand field" describes as the transition from T_{1g} to $^2T_{2g}$. The spectra obtained from all of the samples were similar to each other but different from the spectrum of the P25 that did not undergo heat treatment (WHT). This shifting of the absorption bands is attributed to the temperature (500°C) at which the samples were treated. Increases in the TiO_2 absorption in the visible region caused by the presence of N after subjecting the TiO_2 to higher heat treatments have been reported. This increase is attributed to the oxygen vacancies generated by N removal at high temperatures [23]. Based on the above, and with the knowledge that P25 contains impurities of N, H, C, S and Cl [18], it can be surmised that subjecting the catalysts to a temperature of

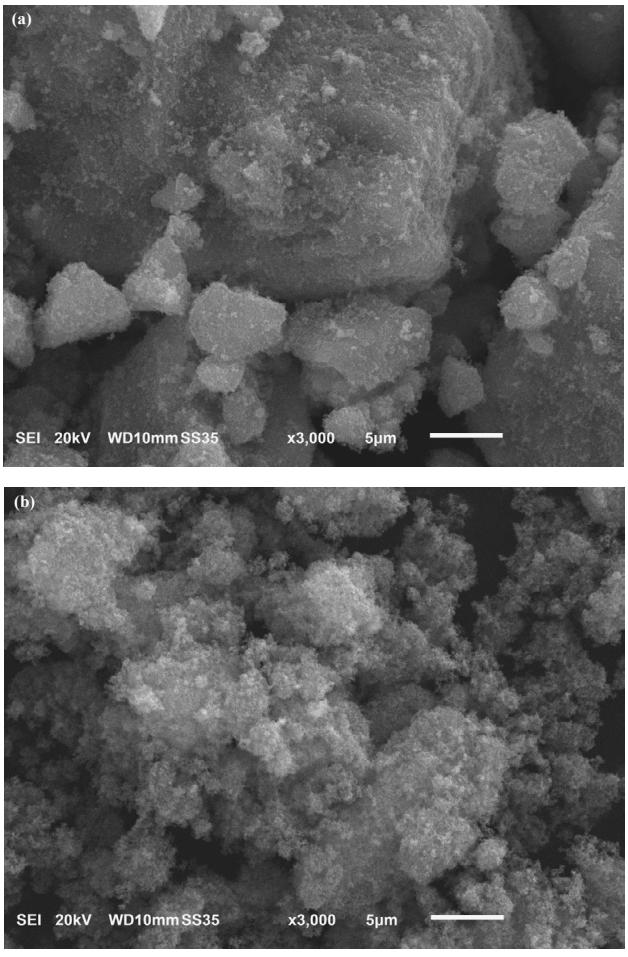

Figure 1: Images obtained by SEM to the TiO_2- P25: a) with thermal treatment and b) without thermal treatment.

500°C will remove the impurities from P25 and increase the oxygen vacancies, which are responsible for increasing the P25 absorption to wavelengths higher than 400 nm. This fact was corroborated with the quantitative analysis of TiO_2-P25 performed by EDS in the MEB. Figure 3 shows the EDS spectra of TiO_2-P25 without heat treatment (a) and calcined at 500°C. It was found that untreated TiO_2-P25 initially contains 6.27 wt% of C and 0.29 wt% of Cl, which matched with that reported previously [18]. By submitting P25 to thermal treatment, the amount of C decreased to 4.44 wt%, and there was no detectable Cl in the sample (see Table 2). Therefore, it was confirmed that the decrease and disappearance of some impurities, such as C-Cl, in the TiO_2 P25 formed oxygen vacancies, which increased P25 absorption in the visible region.

Band gap values, reported in Table 1, for the materials that were submitted to the same treatment conditions had values close to 2.7 eV, whereas untreated P25 had a value of 3.01 eV (Figure 4), which matches with that reported in the bibliography. The conditions under which the catalysts were synthesized decreased the band gap of P25, but insertion of the lanthanide had no effect on the Eg. Additionally, it has been reported that the inclusion of La, Ce, Y, Pr and Sm on the surface of P25 does not diminish Eg, yet the photocatalytic activity is enhanced remarkably [19]. The opposite is true for TiO_2 doped and synthesized via the Sol-Gel method, as under these synthetic conditions the presence of lanthanides as dopants caused a decrease of Eg compared to pure TiO_2 [24].

Photocatalytic degradation variable effects

Table 3 shows the experimental design factors with their respective levels, as well as the treatments obtained by the evaluation of the photocatalytic activity. The generated data satisfied the principles of independence, normality and homoscedasticity. To establish statistically significant differences between the contrasted treatments, multifactorial ANOVA was used, followed by a multiple average Scheffé contrast test. The statistical tests were performed using the Statgraphics Centurion 16.1.15 program.

Catalytic evaluation revealed that aqueous diuron still had a physical absorption balance due to the catalysts after 30 min of the reaction in darkness. This absorption was not present at the end of the reactions, but the presence of hydroxylated surfaces determined by IR spectroscopy indicated that the catalysts were still active and could be reused.

Statistical analysis revealed that only illumination type/mode caused a statistically significant effect both for oxidation and diuron mineralization (multifactorial ANOVA; P<0.01). It was observed that the reactions carried out with solar illumination exhibited improved oxidation (96.97 ± 1.36), though there is only a slight difference (3.36%) in comparison with the UV evaluated reactions (93.62 ± 1.88). The difference in diuron mineralization between the two reactions was larger (12.55%). Therefore, sunlight was the best option for catalytic efficiency in photocatalytic reactions. These data confirmed the results obtained by UV-Vis spectroscopy with diffuse reflectance, which indicated light sources with wavelengths above 400 nm have the highest photocatalytic activity on the impregnated materials.

The rate constants *"k"* for each treatment in the experimental design are presented in Table 3. Figure 5a presents the comparisons between the regression lines of each treatment taking into account diuron's concentration. All treatments start from the same point of origin, as it was established in the statistical analysis that all treatments

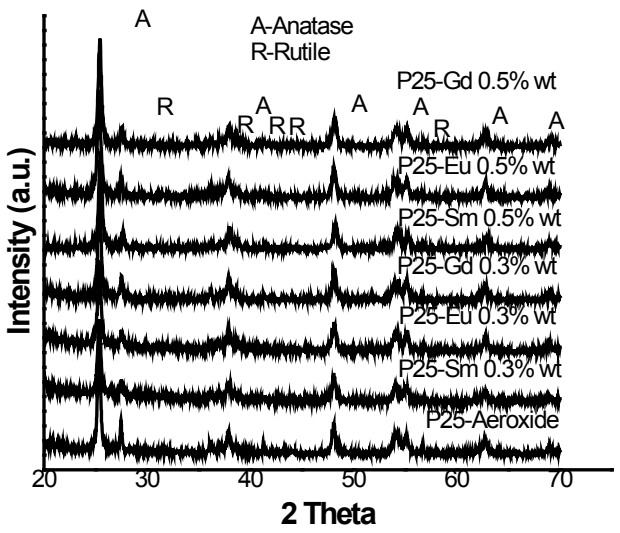

Figure 2: XRD patterns of the catalysts treated at 500°C.

have the same intersection because each experimental unit started from a concentration of 40 mgL^{-1}. It was found that several of the treatments have statistically significant differences (P<0.01), but some treatments (T13, T2, T3, T4 and T6) behave similarly (P>0.05). Treatments were fitted to equation (4), which shows the linear regression model used:

$$\ln\frac{Co}{C} = 0.2680 + 0.0091 \times \text{Reaction Time} \quad (4)$$

This adjusted model explained 93.26% of the variability of $\ln\frac{Co}{C}$, with an estimated standard error of 0.34. The value corresponding to the slope of this model showed us the value of *"k"* for each treatment, and the slope of each treatment varied according to the probability value found. The value of *"k"* was used to determine the half-life ($t_{(1/2)}$) for each treatment, and these are shown in Table 3.

Treatments performed under sunlight showed increased photocatalytic activity with the inclusion of the metals in P25, while, in some cases, UV light treatments had the opposite effect. The addition of metallic impurities in the TiO_2-P25 increases the photocatalytic activity of TiO_2-P25 because they generate higher charge carriers (e^- and h^+). Treatment 12 (T12) was the most active, therefore its $t_{(1/2)}$ was the lowest. A similar case reported by Katsumata et al. [21] for removal of the same contaminant involved insertion of Pt ion into the P25. These results reveal that the improvement of the photocatalytic activity is mainly because the impregnated Pt induces an efficient separation of electron-hole pairs, inhibiting its recombination. In our case, the trivalent ions of Sm, Eu and Gd generated the same effect because the temperature at which they were treated produced a coalescence effect on the surface of P25, generating a superficial charge imbalance that increased charge carriers. According to the theory of semiconductors, ions inserted in this study produced an imbalance of charges, generating an intrinsic semiconductor type "p", which caused an excess of positive charge carriers (h^+) on the TiO_2-P25 particle. When electrons are photo activated by >400 nm light, they are transferred to the conduction band of the inserted ions within P25 and trapped there. According to the claims raised by Saktiaviel et al. [25], this capture is what retards the recombination process e^--h^+ and allows the efficient separation of charges. Because of this, electrons are available to reduce the O_2 present in the reaction, and an excess of h^+ is available to generate and increase

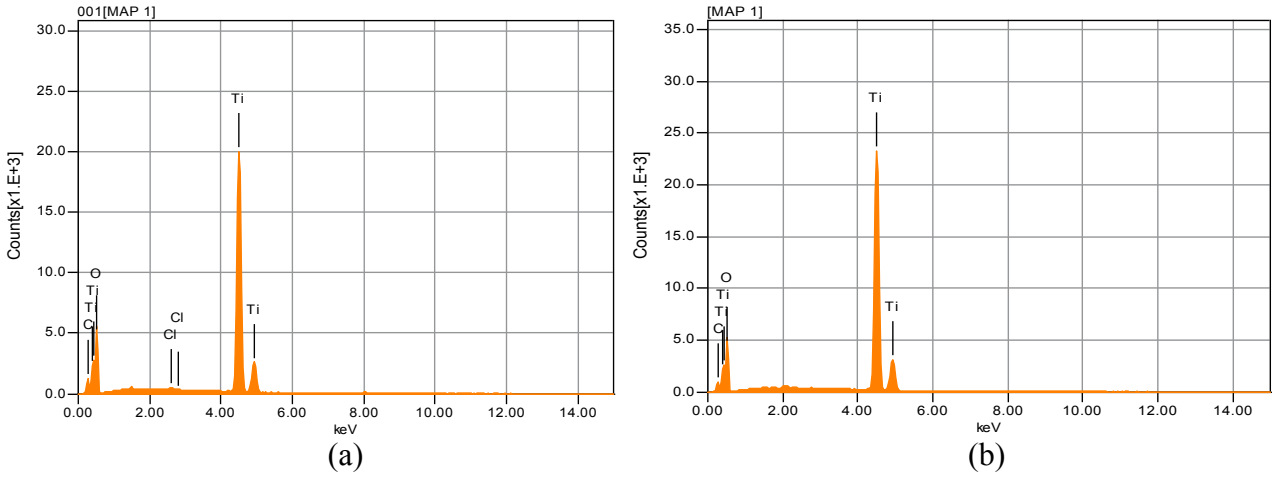

Figure 3: EDS spectra of TiO_2-P25: a) without thermal treatment and b) with thermal treatment.

Sample calcined to 500°C	Surface area (BET)* m^2g^{-1}	Average crystal size for each phase (nm)		Distribution of the mixture crystalline phases		Band gap energy (eV)
		Anatase	Rutile	Anatase	Rutile	
TiO_2-P25	53.17	21.71	85.49	71	29	2.71
P25/Sm 0.3% wt	52.49	21.71	85.49	74	26	2.77
P25/Eu 0.3% wt	52.63	21.71	68.40	76	24	2.71
P25/Gd 0.3% wt	69.49	26.06	85.49	78	22	2.77
P25/Sm 0.5% wt	55.23	21.71	68.40	81	19	2.72
P25/Eu 0.5% wt	51.34	21.71	68.40	80	20	2.74
P25/Gd 0.5% wt	49.98	21.71	68.40	81	19	2.72

Table 1: Results of characterization techniques applied to the catalysts: N_2 physisorption using the BET method, XRD and UV-Vis spectroscopy with reflectance diffuse.

TiO_2-P25 without thermal treatment			TiO_2-P25 calcined at 500°C		
Element	% wt	% mol	**Element**	% wt	% mol
Carbon	6.27	12.25	**Carbon**	4.44	9.19
Oxygen	42.88	62.82	**Oxygen**	39.88	61.93
Chlorine	0.29	0.19	**Chlorine**	0	0
Titanium	50.56	27.74	**Titanium**	55.58	28.88

Table 2: Results of quantitative analysis by EDS realized to the TiO_2-P25 without thermal treatment and to the TiO_2-P25 calcined at 500°C.

the OH^* radicals responsible for oxidizing the contaminant molecule.

The pseudo-constant speed for diuron mineralization was realized using the same comparison of regression lines, shown in Figure 5b. There are statistically significant differences ($P<0.01$) between the treatments compared. The treatments T2, T3, T4, T5, T6 and T12 all behaved similarly ($P>0.05$), whereby, under the conditions established by these treatments, similar effects are obtained. Equation (5) is the linear model that was used to compare treatments:

$$Mineralization\,\% = 10.7091 + 0.2376 \times \text{Time Reaction} \quad (5)$$

The model explained 90.47% of the variability of mineralization % data, with an estimated standard error of 9.82. The highest values of the slopes showed a favorable behavior for each treatment mineralization (pseudo-constant). T9 had the highest value, indicating that under the conditions of this treatment, diuron mineralization developed in a more efficient way. These results are shown in Table 3. With both light sources, there was more activity with catalysts than in control experiments, except T12. This treatment reflected the best reaction kinetics for the oxidation of diuron, but its mineralization was lower than that in T14. However, it was observed that the mineralization between T9 and T12 decreased due to the increase in the concentration of Gd^{3+} on the P25. This indicated that 0.3 wt% Gd^{3+} is the optimal concentration for this metal. This value is very close to that reported by Peng et al. [26], who determined that 0.35 wt% Gd has the highest photocatalytic activity as a dopant in TiO_2. They described that a part of the Gd was incorporated into the crystal lattice of anatase because network parameters were changed, and the rest was distributed superficially forming aggregates or gadolinium nanoparticles. This superficial distribution occurs in this study, due to the preparation method used. The increase of superficial aggregates in the P25 acts as recombination centers for photo-generated charge carriers. Because of this, the photocatalytic activity decreased when concentration of Gd increased. Metal aggregates as dopants on TiO_2 have been described

Factor A: Lighting mode	Factor B: Impregnated metal concentration	Factor C: Impregnated metal	Kinetic constant"*k*" min^{-1}	Half-life "$t_{1/2}$" Min	Mineralization Pseudo-constant min^{-1}	Treatments
UV light (λ=254 nm)	0.3% wt	Sm	0.00909	76.28	0.2376	**1**
		Eu	0.00956	72.50	0.2443	**2**
		Gd	0.00848	81.78	0.2021	**3**
	0.5% wt	Sm	0.00926	74.86	0.2666	**4**
		Eu	0.01056	65.66	0.2730	**5**
		Gd	0.00912	76.00	0.2225	**6**
Solar light (λ>400 nm)	0.3% wt	Sm	0.01331	52.10	0.3116	**7**
		Eu	0.01246	55.61	0.3210	**8**
		Gd	0.01305	53.14	0.3322	**9**
	0.5% wt	Sm	0.01327	52.23	0.3253	**10**
		Eu	0.01360	50.95	0.3258	**11**
		Gd	0.01494	46.40	0.2374	**12**
Witness	TiO_2-P25 UV		0.00966	71.79	0.0984	**13**
Witness	TiO_2-P25 Solar		0.01191	58.18	0.3013	**14**

Table 3: Experimental design used to evaluate the photocatalytic activity of the catalysts synthesized.

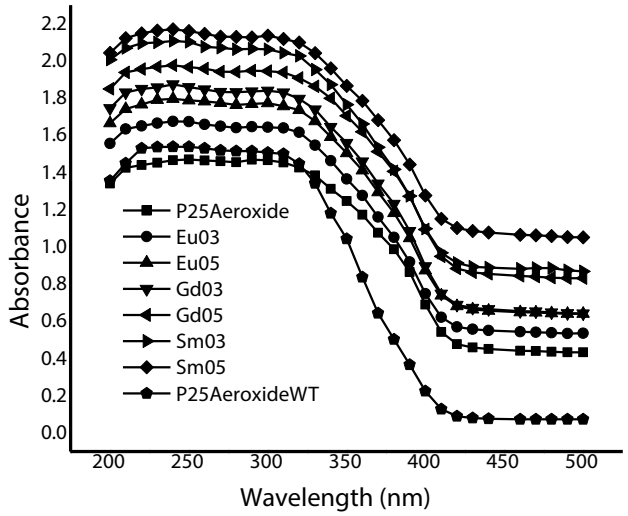

Figure 4: UV-Vis diffuse reflectance spectra of the catalysts synthesized and TiO_2-P25 without heat treatment (WHT).

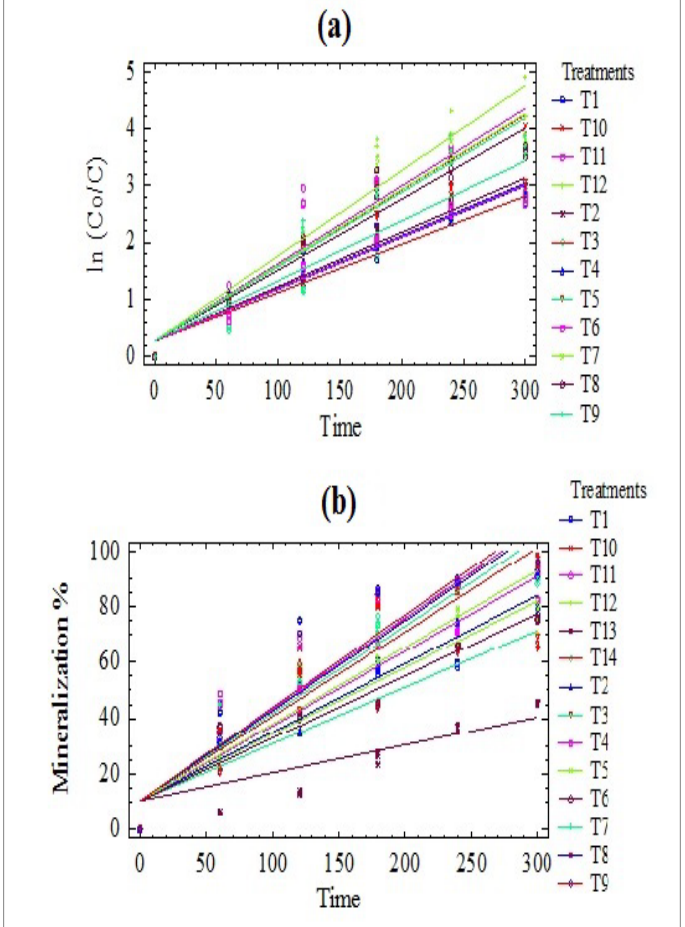

Figure 5: Contrast regression lines because of the diuron oxidation and mineralization of each treatment raised in experimental design with different reaction times.

by Akpan and Hameed [27]; they explain that the increment of these additions increase the electron density around the nucleus, resulting in repulsion of additional electrons that are introduced. The concentration of these electrons around the nucleus provides additional protection and some repulsive forces with Ti, which is not a good interaction. We assume this explains the reduction in P25 photocatalytic activity when the concentration of Gd is increased.

However, increasing the concentration of Sm^{3+} and Eu^{3+} in the TiO_2-P25 caused an increase in activity, though there is a maximum concentration after which the same results as for Gd will occur. This result revealed that the TiO_2-P25 could retain a higher concentration of these metals to manifest a high photoactivity. The main reasons why photocatalytic activity of TiO_2-P25 is increased when it is impregnated with Sm, Eu and Gd are that these lanthanide ions can generate a large

amount of charge carriers, and they have the ability to form complexes with electron donor compounds, which is due to the interaction between their "*f*" orbitals and the functional groups of the electron donor compounds [28].

Conclusion

The catalysts used in this study underwent a heat treatment that removed some impurities, namely C and Cl, generated in the manufacturing process of P25. This generated oxygen vacancies which altered the distribution of the crystalline phases, the electronic and photocatalytic behavior. This decreased the Eg, allowing it to have a higher photoactivity in the visible region. It was demonstrated statistically that the lighting method had the most effect on the photocatalytic process, and sunlight was determined to have the best output. This was corroborated by the values of the Eg of catalysts, which corresponded to λ of the visible region. The inclusion of Sm^{3+}, Eu^{3+}, and Gd^{3+} ions into the TiO_2-P25 increased the photocatalytic activity, due to both the generation of charge carriers and the formation of complexes with diuron. The conditions of experiment T9 were the most efficient for removing diuron from aqueous media. This treatment determined the optimum amount of doped Gd^{3+} needed to increase the activity of P25. A great contribution of the study was showing the activity of the catalysts using the inexhaustible resource of sunlight, which reduces costs incurred by providing an artificial light source for the photocatalytic process.

Nomenclature

K form factor value is 0.9.

M indirect transition between the valence bands and conduction equal to 1.

I_A maximum intensity of the peak corresponding to anatase phase (101).

I_R maximum peak intensity corresponding to the rutile phase (101).

A parameter independent of photon energy for transitions equal to 0.

$Ln\frac{C_o}{C}$ Data transformation of initial and final concentration of Diuron to natural logarithm.

Greek symbols

λ' Wavelength of the radiation used λCu in nm.

λ nm wavelength.

β Mid-height width of the diffraction peak shown in rad. anatase (25.4°) and rutile (27.5°).

α Absorption coefficient equal to 0.

h Planck constant in eVs^{-1}.

θ Diffraction peak position in°.

v Frequency in sec^{-1}.

Acknowledgments

We thank the Universidad Juarez Autónoma de Tabasco and CICTAT, for use of the laboratories of Physicochemical Characterization of Materials, Nanoestructural Catalytics Laboratory and X-ray diffraction of the "División Académica de Ciencias Básicas"; the engineer Anabel González Díaz for performing analysis by SEM; CONACyT grants 31831 and 408259, which was awarded to Juan Carlos Arévalo Pérez for the realization of their postgraduate formation, FOMIX-TAB-2008-C12-91858 and CONACYT-132648 projects.

References

1. Hassal KA (1990) The biochemistry and uses of pesticides: Structure metabolism, mode of action and uses in crop protection. 2nd edn., VCH Verlagsgesellschaft, Weinheim, p: 536.
2. Tomlin C (1997) The pesticide manual. 11th edn. Britihs Crop Protection Council, Farnham Surrey, United Kingdom, pp: 1437-1439.
3. Revitt DM, Ellis JB, Llewelly NR (2002) Seasonal removal of herbicides in urban runoff. Urban Water 4: 13-19.
4. Zhang M, Geng S, Ustin SL, Tanji KK (1997) Pesticide occurrence in groundwater in Tulare county, California. Environmental Monitoring Assessment 45: 101-127.
5. Malato S, Blanco J, Vidal A, Alarcon D, Maldonado MI, et al. (2003) Applied studies in solar photocatalytic detoxification: an overview. Solar Energy 75: 329-336.
6. Carrier M, Besson M, Guillard C, Gonze E (2009) Removal of herbicide diuron and thermal degradation products under catalytic wet air oxidation conditions. Applied Catalysis B: Environmental 91: 275-283.
7. Zhang J, Zheng Z, Zhao T, Zhao Y, Wang L, et al. (2008) Radiation-induced reduction of diuron by gamma-ray irradiation. Journal of Hazardous Materials 151: 465-472.
8. Bouras O, Bollinger JC, Baudu M, Khalaf H (2007) Adsorption of diuron and its degradation products from aqueous solution by surfactant-modified pillared clays. Applied Clay Science 37: 240-250.
9. Bazot S, Bois P, Joyeux C, Lebeau T (2007) Mineralization of diuron [3-(3,4-dichlorophenyl)-1, 1-dimethylurea] by coimmobilized Arthrobacter sp. and Delftia acidovorans. Biotechnology Letters 29: 749-754.
10. Malato S, Caceres J, Fernandez AR, Piedra L, Hernando MD, et al. (2003) Photocatalytic Treatment of Diuron by Solar Photocatalysis: Evaluation of Main Intermediates and Toxicity. Environmental Science and Technology 372: 2516-2524.
11. Fujishima A, Rao TN, Donald TA (2000) Titanium dioxide photocatalysis. Journal of Photochemistry and Photobiology C: Photochemistry Reviews 1: 1-21.
12. Stengl V, Bakardjieva S, Murafa N (2009) Preparation and photocatalytic activity of rare earth doped TiO_2 nanoparticles. Materials Chemistry and Physics 114: 217-226.
13. Xu AW, Gao Y, Liu HQ (2002) The preparation, characterization, and their photocatalitic activities of rare earth doped TiO_2 nanoparticles. Journal of Catalysis 207: 151-157.
14. Parida KM, Sahu N (2008) Visible light induced photocatalytic activity of rare earth titania nanocomposites. Journal of Molecular Catalysis A: Chemical 287: 151-158.
15. Ghosh S, Divya D, Remani KC, Sreeremya TC (2010) Growth of monodisperse nanocrystals of cerium oxide during synthesis and annealing. Journal of Nanoparticle Research 12: 1905-1911.
16. Spurr RA, Myers H (1957) Quantitative Analysis of Anatase-Rutile Mixtures with an X-Ray Diffractometer. Analytic Chemistry 29: 760-762.
17. Datye AK, Riegel G, Bolton JR, Huang M, Prairie MR (1995) Microstructural Characterization of a Fumed Titanium Dioxide Photocatalyst. Journal of Solid State Chemistry 115: 236-239.
18. Ettlinger M (1995) Highly Dispersed Metallic Oxides Produced by the AEROSIL® Process. Degussa's Technical Bulletin Pigments 56, Frankfurt, Germany.
19. Du P, Bueno AL, Verbaas M, Almeida AR, Makkee M (2008) The effect of surface OH^- population on the photocatalytic activity of rare earth-doped P25-TiO_2 in methylene blue degradation. Journal of Catalysis 260: 75-80.
20. Ying JY, Zhang Z, Wang CC, Zakaria R (1998) Role of Particle Size in Nanocrystalline TiO_2-Based Photocatalysts. Journal of Physical Chemistry B 102: 10871-10878.
21. Katsumata H, Sada M, Nakaoka Y, Kaneco S, Suzuki T, et al. (2009) Photocatalytic degradation of diuron in aqueous solution by platinized TiO_2. Journal of Hazardous Materials 171: 1081-1087.
22. Mogyorosi K, Vereb G, Ambrus Z, Pap Z, Kmetyko A, et al. (2012) Comparative study on UV and visible light sensitive bare and doped titanium dioxide

photocatalysts for the decomposition of environmental pollutants in water. Applied Catalysis A: General, pp: 417-418.

23. Yamada K, Yamane H, Matsushima S, Nakamura H, Ohira K (2008) Effect of thermal treatment on photocatalytic activity of N-doped TiO_2 particles under visible light. Thin Solid Films 516: 7482-7487.

24. Laz CD, Arevalo JC, Torres G, Bautista RG, Ornelas C, et al. (2011) TiO_2 Doped with Sm^{3+} by sol-gel: synthesis, characterization and photocatalytic activity of Diuron under solar light. Catalysis Today 166: 152-158.

25. Sakthivel S, Shankar MV, Palanichamy M, Arabindoo B, Bahnemann DM, et al. (2004) Enhancement of photocatalytic activity by metal deposition: characterisation and photonic efficiency of Pt, Au and Pd deposited on TiO_2. Water Research 38: 3001-3008.

26. Peng T, Zhao D, Liu M, Lu L, Cai P (2008) Fabrication, charactherization and photocatalytic activity of Gd^{3+} doped titania nanoparticles with mesostructure. Microporous and Mesoporous Materials 114: 166-174.

27. Akpan UG, Hameed HB (2010) The advancements in Sol-Gel method of doped-TiO_2 photocatalyst. Applied Catalyst A: General 375: 1-11.

28. Wang Y, Cheng H, Zhang L, Hao Y, Ma J (2000) The preparation, characterization, photoelectrochemical and photocatalytic properties of lanthanide metal-ion-doped TiO_2 nanoparticles. Journal of Molecular Catalysis A: Chemical 151: 205-216.